Supplemental Materials

Molecular Biology of the Cell

Hummert *et al*.

ALGORITHM AND BENCHMARKING

The preliminary step detection (part two in the framework, detailed in the main text) relies on the algorithm developed by Kalafut and Vischer (Kalafut and Visscher, 2008), which uses the Schwarz Information Criterion (SIC) to evaluate steps. In this context the SIC is defined as:

$$SIC(j_1, \dots, j_k) = (k+2)log(n) + n \ln \widehat{\sigma}^2_{j_1,\dots,j_k} + n \ln 2\pi + n$$

Steps are successively added until the addition of the step does not improve the SIC further. In the modified version used here steps where the difference in means, i.e. the mean signal before and after the added step, is below a defined threshold parameter, are not added even if they improve the SIC.

The step refinement (part IV in the framework, detailed in the main text) relies on the posterior from Pressé et al. (Tsekouras et al., 2016):

$$\begin{aligned} -2\ln P(\theta|D) = & \sum_{\phi=0}^{K} \left(n_\phi \ln\left(i\sigma_f^2 + \sigma_b^2\right) + \sum_{l=1}^{n_\phi} \left(\frac{x_l - i\mu_f - \mu_b}{i\sigma_f^2 + \sigma_b^2}\right)\right. \\ & + 2\left(-K\ln\lambda - \ln\left((m-K)!\right) - \ln K! - \ln(m-1)! + \sum_{y=0}^{m-K} \ln d_y!\right) \\ & + 2\left(\gamma_0 \frac{m-K+1}{K} + \ln(m-K+2) + \ln(m-K+1) - \ln(m-K+2)\right. \\ & \left.\left. - (m-K+1)e^{-\gamma_0/K}\right)\right) \end{aligned}$$

This expression is minimized iteratively, with fixed hyperparameters, using the algorithm in the flowchart (Figure 2b in the manuscript).

SUPPORTING TABLES

Table S1

Spectroscopic properties of fluorophores used. Properties determined in PBS, pH 7.4-7.5 unless stated otherwise. ε extinction coefficient, ϕ fluorescence quantum yield, λ_{peak} peak absorption wavelength, λ_{ex} excitation wavelength. Spectral correction factors (CF_λ) were determined from published spectra or spectra measured for unconjugated BG/HA-dyes.

Fluorophore	ε [x10^3 M^{-1}cm^{-1}]	ϕ_{fl}	λ_{peak} [nm]	λ_{ex} [nm]	CF_λ	Primary ref.
EGFP	55.9	0.6	488	488	0.62	Cormack et al. (1996)
mNeonGreen	116	0.8	506	488	1.0	Shaner et al. (2013)
mCherry	72	0.22	587	561	0.64	Shaner et al. (2004)
BG-TMR	89[a,f]	0.39[b,g]	555[f]	561	0.86	Keppler et al. (2003)
BG-SiR	43.2[c,g]	0.30[b,g]	650[g]	640	0.75	Lukinavicius et al. (2013)
HTL-TMR	78[d,f]	0.41[d,f]	548[f]	561	0.89	Los et al. (2008)
HTL-SiR	130.2[c,g]	0.39[b,g]	648[g]	640	0.71	Lukinavicius et al. (2013)
ATTO 647N	150[e]	0.65[e]	646	640	0.92	ATTO-TEC

[a] (Keppler et al., 2006)

[b] (Lukinavičius et al., 2013)

[c] (Erdmann et al., 2019)

[d] Tetramethylrhodamine, (Grimm et al., 2015)

[e] ATTO-TEC data sheet available at https://www.atto-tec.com

[f] Free dye

[g] Protein conjugate

Table S2

Symbols used

SIC	
$j_1, \ldots, j_k$	Step positions
n	Timepoints in the trace
$\hat{\sigma}^2$	Sum over the variances of data between steps
Posterior	
θ	Bayesian parameters
D	Data (photobleaching trace)
K	Number of steps
n_ϕ	Timepoints in interval ϕ
σ_f	Standard deviation of the single fluorophore signal
σ_b	Standard deviation of the background signal
x_l	Signal at timepoint l
i	Active number of fluorophores at timepoint
μ_f	Mean signal of a single fluorophore
μ_b	Mean background signal
λ	Poisson distribution parameter for event occurrences
m	Number of events (single fluorophore switches)
d_y	Number of data points between steps
γ_0	Cutoff for the hyperparameter constraining K to m

SUPPORTING FIGURES

Figure S1

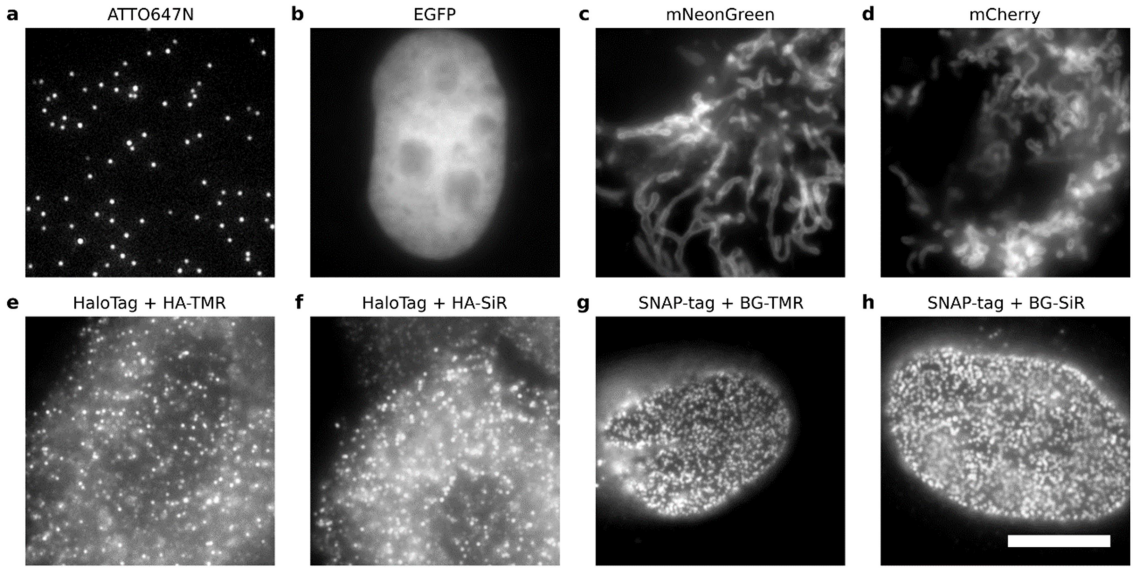

Representative images from samples used for photostability characterization. **a,** DNA-conjugated and surface-immobilized ATTO-647N. **b,** COS-7 cells transiently expressing histone 2A (H2A-EGFP-HaloTag). **c,** COS-7 cells transiently expressing mNeonGreen-TOMM20. **d,** COS-7 cells transiently expressing TOMM20-mCherry-HaloTag. **e,f,** HeLa cells stably expressing GlnA-HaloTag. Cells were labeled with 100 nM HTL-TMR (e) or HTL-SiR (f) for 120 min. **g,h,** U2OS cells stably expressing NUP107-SNAP-tag were labeled with 200 nM BG-TMR (g) or BG-SiR (h) for 120 min. Representative images from 2 independent experiments per condition are shown. Scale bar: 10 µm.

Figure S2

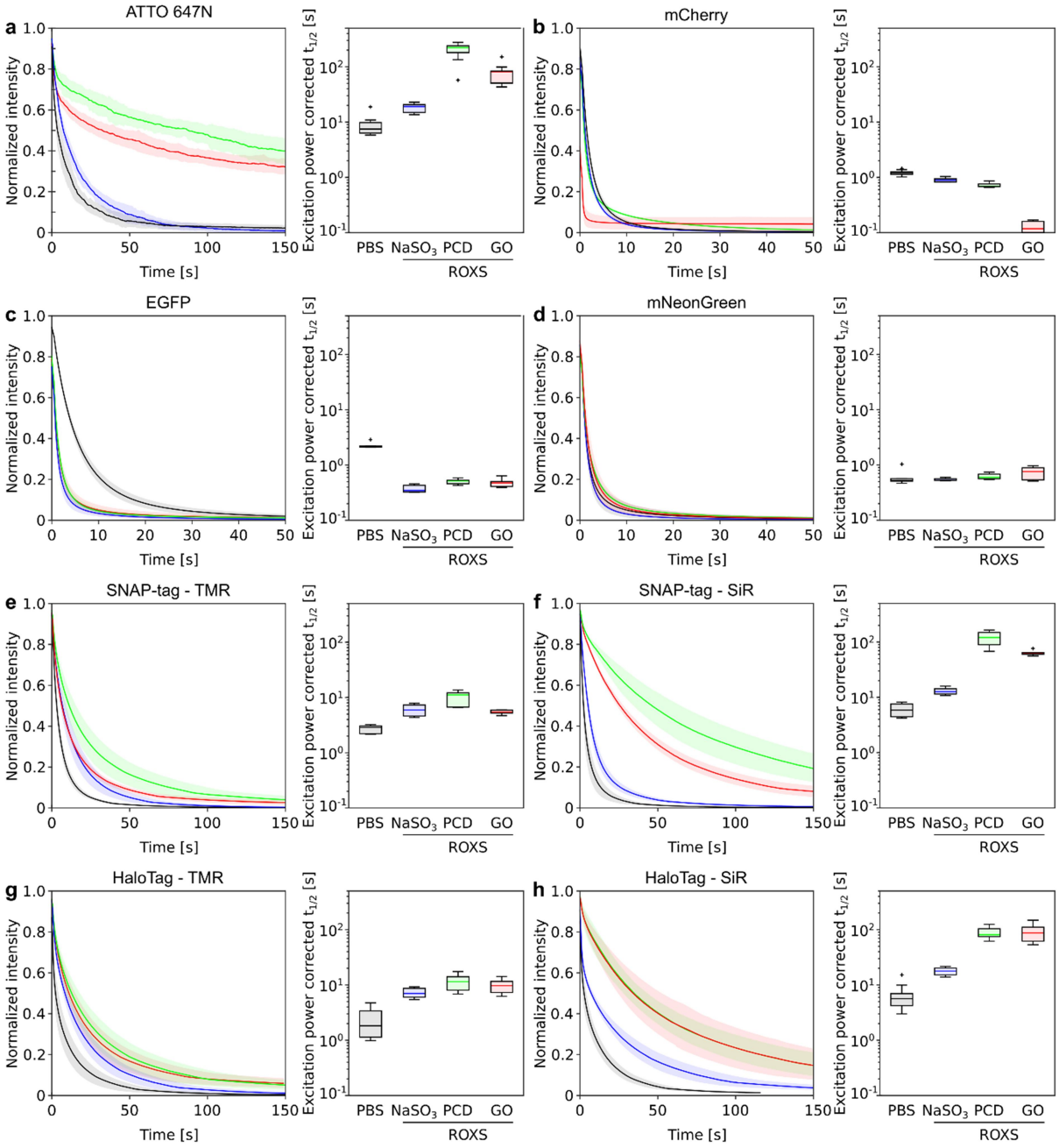

Photostability measurements for fluorescent proteins and protein tag substrates. Each fluorophore was exposed to high intensity illumination in respective buffers. Left: Photobleaching curves upon illumination for different buffers. Colors as in box plots. Mean (line)±SD (shaded region) from 7-10 measurements from 2 independent experiments per condition. Right: Corresponding $t_{1/2}$ corrected for excitation power density. Box plots indicate median, 25th and 75th percentiles. Whiskers extend to 1x interquartile range, outliers are plotted as crosses. **a,** 9 (PBS) or 10 (all other conditions) measurements per condition. **b,** 10 measurements per condition. **c,** 10

(PBS), 7 ($NaSO_3$), 9 (ROXS PCD and ROXS GodCat) per condition. **d,** 10 (PBS, ROXS PCD) or 9 ($NaSO_3$, ROXS GodCat) per condition. **e,** 9 (PBS) or 10 (all other conditions) measurements per condition. **f,** 9 (ROXS GodCat) or 10 (all other conditions) measurements per condition. **g,h,** 10 measurements per condition.

Figure S3

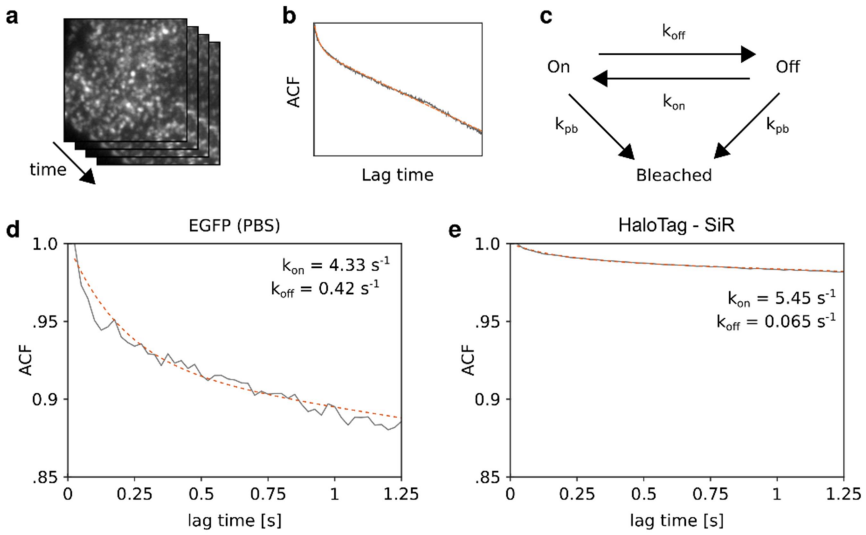

Principle of image correlation-based characterization of photoblinking. a, An image time series recorded showing blinking fluorophores is used as input data. **b**, The temporal autocorrelation function (ACF) is computed according to routine described in (Sehayek et al., 2019). **c**, A 3-state model with a fluorescent on-state, a non-fluorescent off-state and a non-fluorescent bleached state with reversible transitions between on- and off-state and irreversible transition into the bleach state is fitted to ACF. **d,e**, Representative fits (orange, dashed) and raw ACFs (grey) for fluorophore-buffer combinations exhibiting strong photoblinking (d) and weak photoblinking (e). Fitted rates are given for each fit.

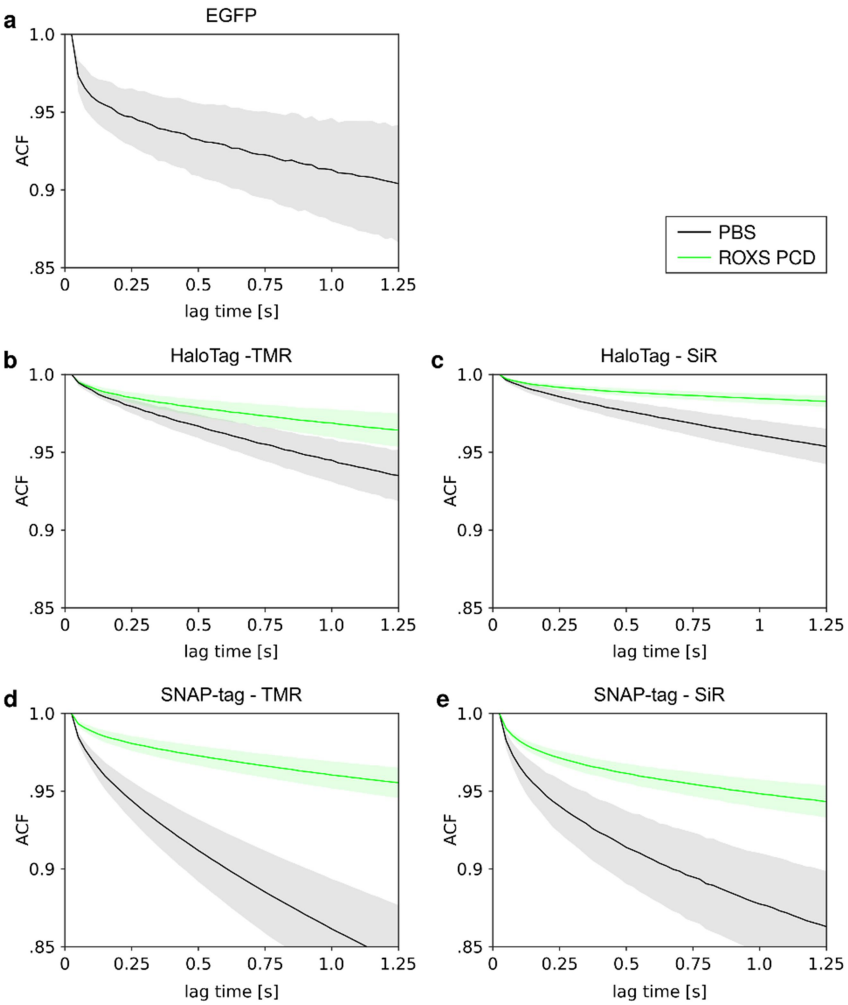

Figure S4 Averaged (lines) ±SD (shaded region) ACFs for indicated fluorophores in PBS (black) or ROXS PCD buffer (green). Averages from 22-54 measurements from 2-4 independent experiments per condition.

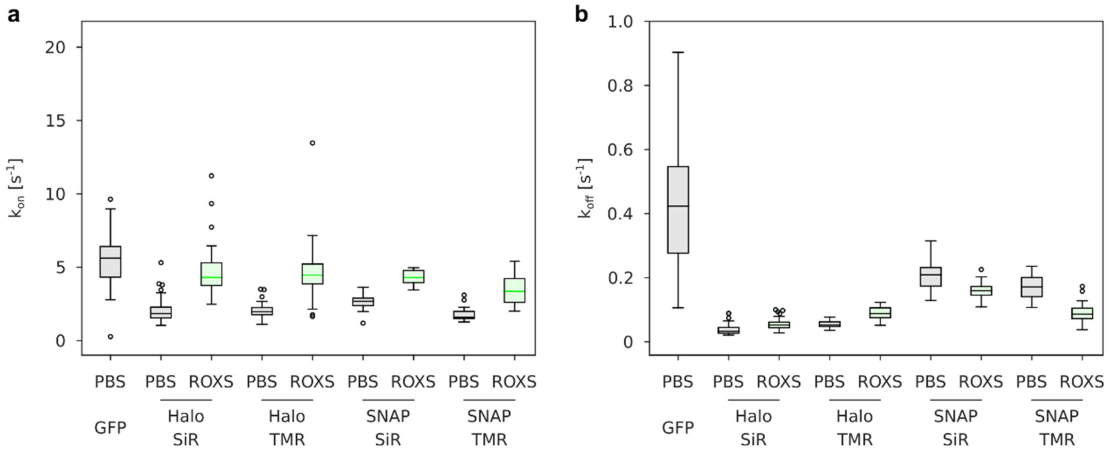

Figure S5 Fluorophore on- (**a**) and off-rates (**b**) for photoblinking between fluorescent and non-fluorescent state in 3-state fluorophore model obtained from fitting of ACFs.

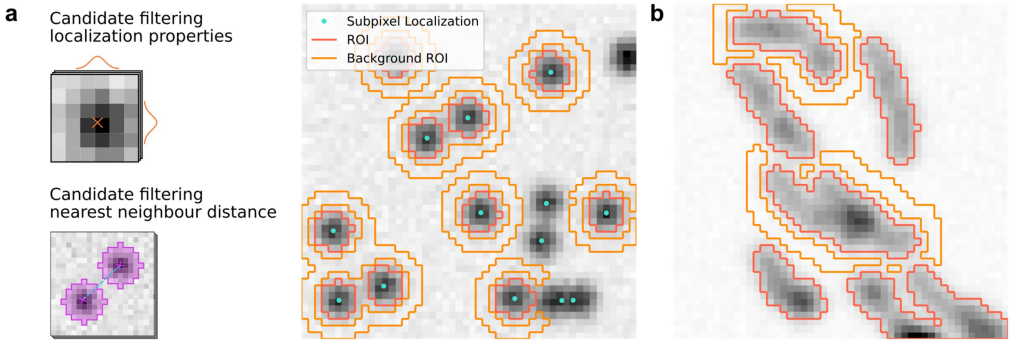

Figure S6 Trace extraction routines included in the quickPBSA package shown schematically on artificial data. **a**, Extraction based on localization coordinates. Diffraction limited spots are excluded based on nearest neighbor distance and localization parameters such as width. **b**, Extraction based on a mask image. Overlap with other ROIs is excluded from background ROIs. ROIs can be excluded based on the ROI area.

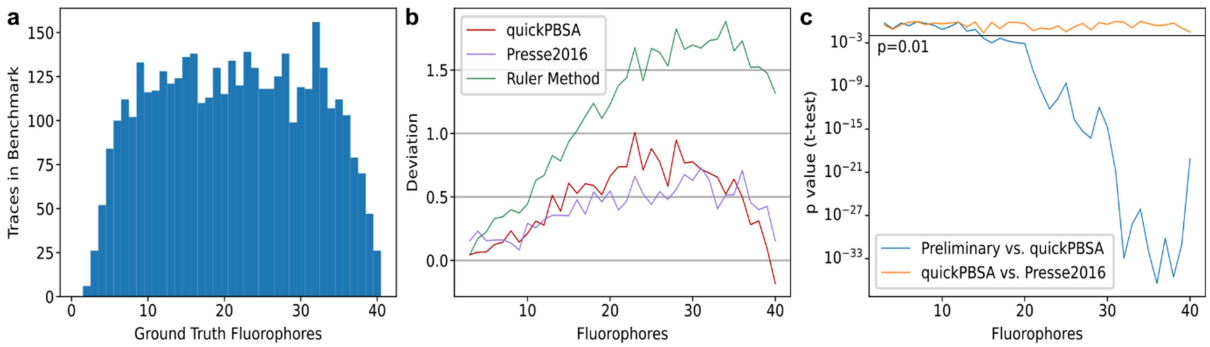

Figure S7 Benchmarking of quickPBSA and comparison with alternative approaches. **a,** Histogram of the number of synthetic traces included in the benchmark for each ground-truth fluorophore number. **b**, Deviation of fluorophore number estimate with quickPBSA and Presse2016 compared to a simple ruler method. The ruler method compares the height of the last step with the intensity at the beginning of the trace. **c**, t-test result comparing the means extracted with quickPBSA to the results of Presse2016 and the result of the presented algorithm without the quickPBSA refinement step.

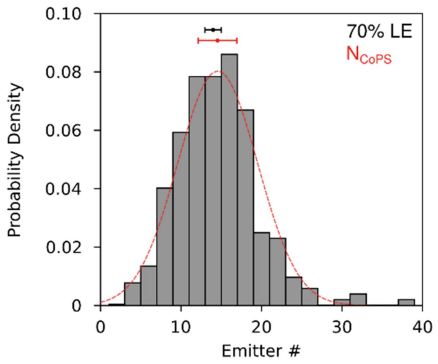

Figure S8 Characterization of R20 DNA origami by CoPS. R20 DNA origami were immobilized as described above and imaged in ROXS PCD buffer supplemented with 10 mM $MgCl_2$. CoPS emitter number estimates from 386 origami. Distribution was modeled with a Gaussian function (dashed red line). Mean±SD from CoPS measurements (black) and from binomial distribution assuming 70% LE (red) shown as dot and horizontal bars above distribution.

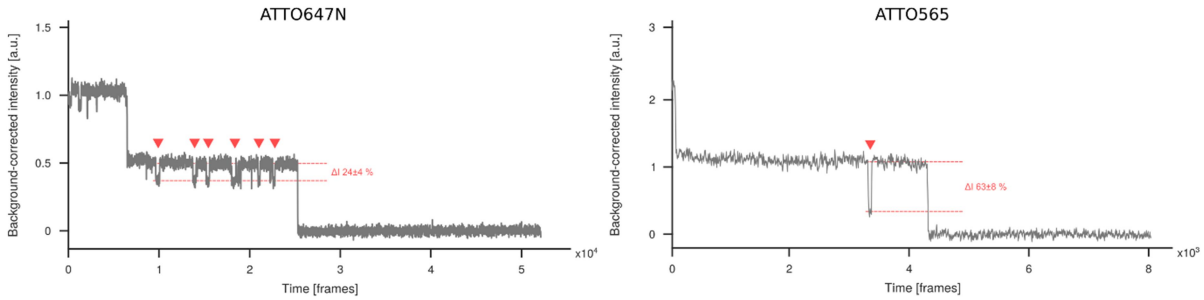

Figure S9 Representative photobleaching traces from the measurements with ATTO 647N and ATTO 565 illustrating the impact of fluorophore properties on photobleaching measurements. The second bright state of ATTO 647N is similar in brightness and does not affect the measurement strongly. In contrast the second bright state of ATTO 565 has a much lower brightness and could explain the overestimation observed in the *in vitro* measurement (Figure 3 in the manuscript).

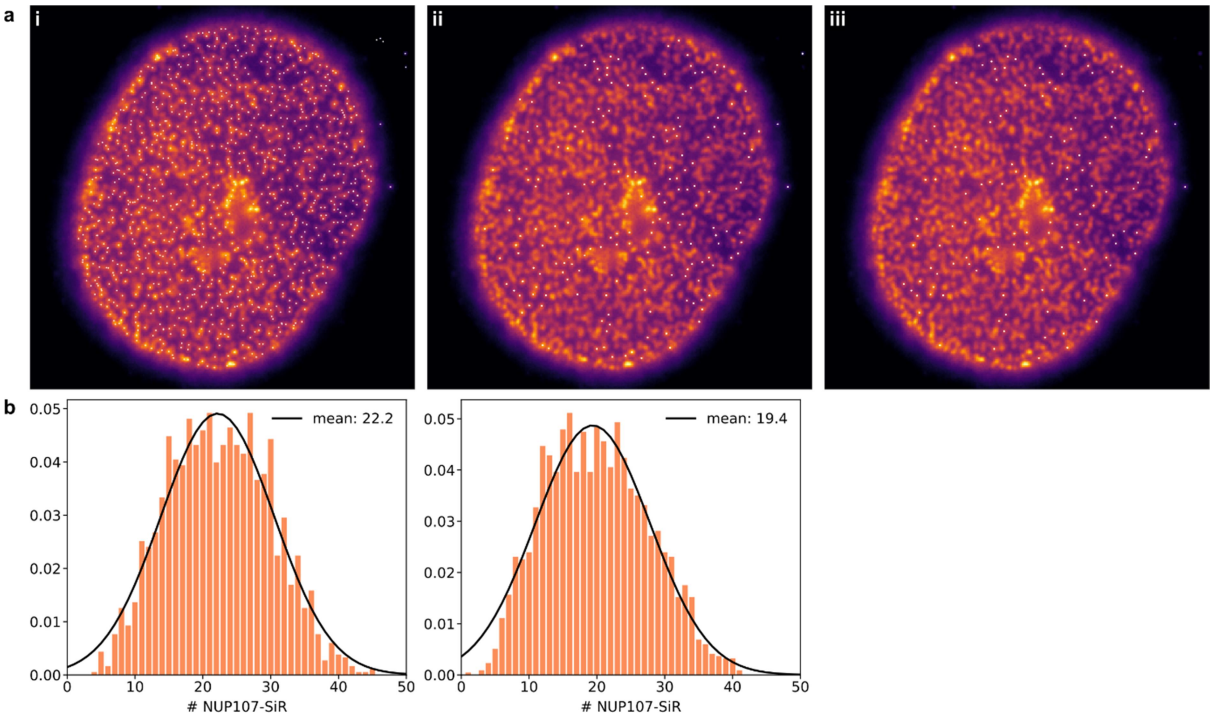

Figure S10 Counting of NUP107. **a,** Representative image with point localization and trace extraction. i) Initial thunderSTORM localization result. ii) Remaining points after density filtering and filtering over Gaussian width from localization. iii) Successfully evaluated spots (not flagged out, see quickPBSA package documentation). **b,** Extracted fluorophore number distributions from the two independent measurements with 15 and 17 cells per experiment, respectively.

SUPPLEMENTAL REFERENCES

Erdmann, R.S., Baguley, S.W., Richens, J.H., Wissner, R.F., Xi, Z., Allgeyer, E.S., Zhong, S., Thompson, A.D., Lowe, N., Butler, R., Bewersdorf, J., Rothman, J.E., Johnston, D.S., Schepartz, A., Toomre, D., 2019. Labeling Strategies Matter for Super-Resolution Microscopy: A Comparison between HaloTags and SNAP-tags. Cell Chem. Biol. 26, 584-592.e6. https://doi.org/10.1016/j.chembiol.2019.01.003

Grimm, J.B., English, B.P., Chen, J., Slaughter, J.P., Zhang, Z., Revyakin, A., Patel, R., Macklin, J.J., Normanno, D., Singer, R.H., Lionnet, T., Lavis, L.D., 2015. A general method to improve fluorophores for live-cell and single-molecule microscopy. Nat. Methods 12, 244–250. https://doi.org/10.1038/nmeth.3256

Kalafut, B., Visscher, K., 2008. An objective, model-independent method for detection of non-uniform steps in noisy signals. Comput. Phys. Commun. 179, 716–723. https://doi.org/10.1016/j.cpc.2008.06.008

Keppler, A., Arrivoli, C., Sironi, L., Ellenberg, J., 2006. Fluorophores for live cell imaging of AGT fusion proteins across the visible spectrum. BioTechniques 41, 167–175. https://doi.org/10.2144/000112216

Lukinavičius, G., Umezawa, K., Olivier, N., Honigmann, A., Yang, G., Plass, T., Mueller, V., Reymond, L., Corrêa Jr, I.R., Luo, Z.-G., Schultz, C., Lemke, E.A., Heppenstall, P., Eggeling, C., Manley, S., Johnsson, K., 2013. A near-infrared fluorophore for live-cell super-resolution microscopy of cellular proteins. Nat. Chem. 5, 132–139. https://doi.org/10.1038/nchem.1546

Sehayek, S., Gidi, Y., Glembockyte, V., Brandão, H.B., François, P., Cosa, G., Wiseman, P.W., 2019. A High-Throughput Image Correlation Method for Rapid Analysis of Fluorophore Photoblinking and Photobleaching Rates. ACS Nano 13, 11955–11966. https://doi.org/10.1021/acsnano.9b06033

Tsekouras, K., Custer, T.C., Jashnsaz, H., Walter, N.G., Pressé, S., 2016. A novel method to accurately locate and count large numbers of steps by photobleaching. Mol. Biol. Cell 27, 3601–3615. https://doi.org/10.1091/mbc.e16-06-0404